Pattern Recognition 44 (2011) 55–69

Contents lists available at ScienceDirect

Pattern Recognition

journal homepage: www.elsevier.com/locate/pr

Clustering ellipses for anomaly detection

Masud Moshtaghi [a,e,*], Timothy C. Havens [b], James C. Bezdek [a,b], Laurence Park [c], Christopher Leckie [a,e], Sutharshan Rajasegarar [d], James M. Keller [b], Marimuthu Palaniswami [d]

[a] Department of Computer Science and Software Engineering, University of Melbourne, Parkville, Melbourne, Australia
[b] Department of Electrical and Computer Engineering, University of Missouri, Columbia, MO 65211, USA
[c] School of Computing and Mathematics, University of Western Sydney, Australia
[d] Department of Electrical and Electronic Engineering, University of Melbourne, Parkville, Melbourne, Australia
[e] NICTA Victoria Research Laboratories, Australia

ARTICLE INFO

Article history:
Received 10 May 2010
Received in revised form
28 June 2010
Accepted 25 July 2010

Keywords:
Cluster analysis
Elliptical anomalies in wireless sensor networks
Reordered dissimilarity images
Similarity of ellipsoids
Single linkage clustering
Visual assessment

ABSTRACT

Comparing, clustering and merging ellipsoids are problems that arise in various applications, e.g., anomaly detection in wireless sensor networks and motif-based patterned fabrics. We develop a theory underlying three measures of similarity that can be used to find groups of similar ellipsoids in p-space. Clusters of ellipsoids are suggested by dark blocks along the diagonal of a *reordered dissimilarity image* (RDI). The RDI is built with the recursive iVAT algorithm using any of the three (dis) similarity measures as input and performs two functions: (i) it is used to visually assess and estimate the number of possible clusters in the data; and (ii) it offers a means for comparing the three similarity measures. Finally, we apply the single linkage and CLODD clustering algorithms to three two-dimensional data sets using each of the three dissimilarity matrices as input. Two data sets are synthetic, and the third is a set of real WSN data that has one known second order node anomaly. We conclude that focal distance is the best measure of elliptical similarity, iVAT images are a reliable basis for estimating cluster structures in sets of ellipsoids, and single linkage can successfully extract the indicated clusters.

1. Introduction: clustering and ellipsoids

Hyperellipsoids (more simply, ellipsoids) occur in many areas of applied mathematics. For example, level sets of Gaussian probability densities are ellipsoids [1]. Ellipsoids also appear often in clustering [2–4] and classifier design [1,5–7]. Please be careful to distinguish the present work, wherein the *input* data objects are ellipsoids, from clustering algorithms such as that of Dave and Patel [4], where the *output* of clustering input sets of object vectors in p-space results in ellipsoidal prototypes.

The application that motivates the present work is the use of ellipsoids for anomaly detection. This problem occurs, for example, in *wireless sensor networks* (WSNs) [8–12] and motif-based patterned fabric defect detection [13]. In particular, the authors of [10] model the data collected at individual sensor nodes by sample-based ellipsoids; in [11] they develop a method for clustering sets of ellipsoids in this context; and in [12] visual tendency of assessment is used to establish the possible presence of clusters of ellipsoids. For example, Fig. 1 is a plan view of the 54 node IBRL (Intel Berkeley Research Lab) WSN installed on March 1, 2004.

Fig. 2 is a set of ellipses generated by summarizing data collected at the 54 nodes of the IBRL. This data is available at the IBRL-Website: http://db.lcs.mit.edu/labdata/labdata.html. The data used in this paper were collected from 8:00 AM to 8:00 PM from the first 18 days of March in 2009. The data consist of 668,830 (t=temperature, h=humidity) pairs, each pair labeled as being collected at one of the 54 nodes. The cardinality for each of the 54 data sets was not quite the same because some of the sets had a few values missing. We conditioned the data by first rounding up the (t, h) values, and then removing duplicate vectors. Each duplicate was weighted by the number of times duplicated, resulting in a total of 8503 weighted pairs. Finally, the sample mean and sample covariance matrix of the vectors associated with each node resulted in the set of 54 ellipses as shown in Fig. 2. We call this data set E54. During this collection period, node 17 showed abnormal behavior, as manifested by the visually apparent "more horizontal" ellipse that stands in stark contrast to the other 53 ellipses. This is a real data example of a second order WSN anomaly as defined in [10–12].

The data in Fig. 2 offer a glimpse of our objectives in this article. First, we develop three measures of similarity for pairs of ellipsoids that (in principle) enable us to look for clusters of ellipsoids. Second, we image reordered versions of the dissimilarity matrices induced on ellipsoidal pairs by the similarity measures with the recursive iVAT algorithm [14,15]. The images

* Corresponding author.
E-mail address: masud.moshtaghi@computer.org (M. Moshtaghi).

0031-3203/$ - see front matter © 2010 Elsevier Ltd. All rights reserved.
doi:10.1016/j.patcog.2010.07.024

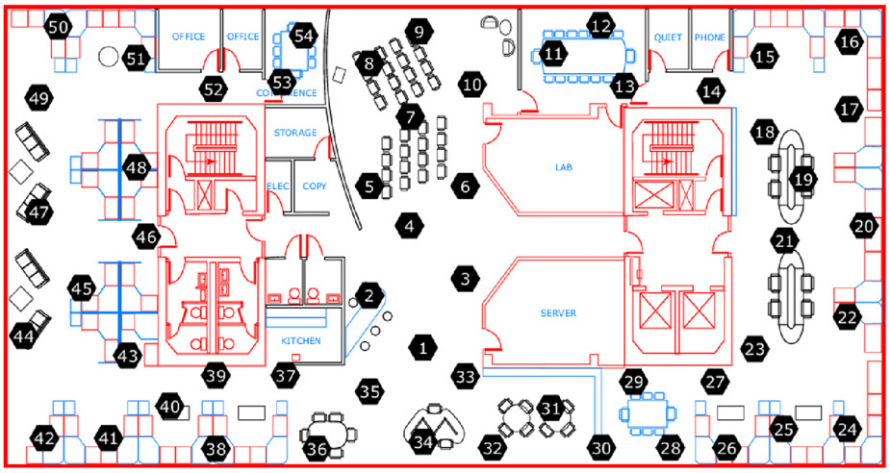

Fig. 1. The IBRL wireless sensor network.

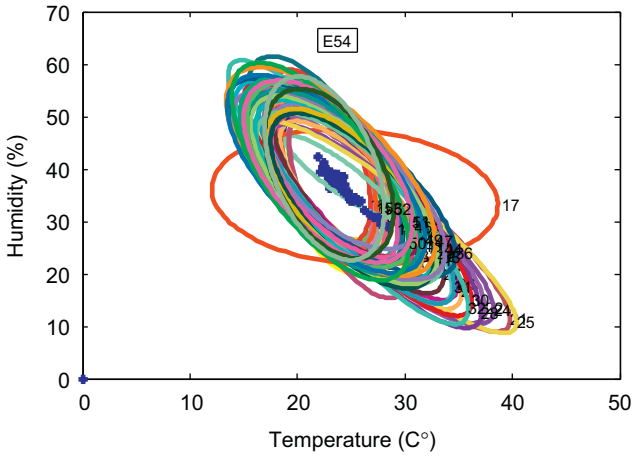

Fig. 2. Ellipsoidal summaries for 54 nodes in the IBRL: node 17 is the visually anomalous ellipse.

are used to assess whether or not the data do contain clusters, and if so, how many? Using estimates of c, the number of clusters in the data found by iVAT and a method based on the ordered eigenvalues of D, we find "optimal" clusters with the *single linkage* (SL, [16]) and CLODD [37] clustering algorithms. Ideally, anomalies in the sets of ellipsoids will not be grouped with (sets of) typical ellipsoids. We will illustrate this procedure with three numerical examples that use both real and artificial WSN data.

This paper is organized as follows. Section 2 reviews the essential algebra and geometry of ellipsoids. Sections 3, 4, and 5 contain definitions and proofs for three measures of similarity or dissimilarity on pairs of ellipses: *compound normal* and *transformation energy* similarities, and *focal distance* dissimilarity. Section 6 discusses the recursive iVAT algorithm for displaying reordered dissimilarity images. Section 7 presents iVAT images for the three data sets we use to illustrate our method. Section 8 discusses clustering in the dissimilarity data produced by each measure with the SL and CLODD algorithms. Section 9 offers our conclusions and some ideas for future research.

2. Similarity measures for pairs of ellipsoids

Let vectors $\mathbf{x},\mathbf{m} \in \Re^p$, and let $A \in \Re^{p\times p}$ be positive definite. The quadratic form $Q(\mathbf{x}) = \mathbf{x}^T A\mathbf{x}$ is also positive definite, and for fixed $\mathbf{m} \in \Re^p$, the level set of $Q(\mathbf{x}-\mathbf{m}) = (\mathbf{x}-\mathbf{m})^T A(\mathbf{x}-\mathbf{m}) = \|(\mathbf{x}-\mathbf{m})\|_A^2$, for scalar $t^2 > 0$, is

$$E(A,\mathbf{m};t) = \{\mathbf{x} \in \Re^p \,|\, \|\mathbf{x}-\mathbf{m}\|_A^2 = t^2\} \tag{1}$$

Geometrically, $E(A,\mathbf{m};t)$ is the (surface of the) hyper-ellipsoid in p-space induced by A, all of whose points are the constant A distance (t) from its center $\mathbf{m}$. Sometimes t is called the "effective radius" of $E(A,\mathbf{m};t)$. When $A=I_p$, $E(A,\mathbf{m};t)$is the surface of a hyper-sphere with radius t. Henceforth, we may omit the prefix "hyper", using ellipsoid and sphere for all cases, $p \geq 2$. Eq. (1) defines an infinite family $\{E(A,\mathbf{m};t) : t > 0\}$ of concentric ellipsoids parameterized in t. Each member of this family can be normalized, $\|\mathbf{x}-\mathbf{m}\|_{A/t^2}^2 = 1$. This simply shifts attention to the scaling of A ($A/t^2 \leftarrow A$) without loss of generality.

Suppose we have two ellipsoids in p-space, E_i and E_j, that have effective radii t_i and t_j, centers [means] $\mathbf{m}_i$ and $\mathbf{m}_j$ and [inverse of covariance] matrices A_i and A_j. First, normalize E_i and E_j, $A_i/t_i^2 \leftarrow A_i$ and $A_j/t_j^2 \leftarrow A_j$. We want a measure of similarity between the two ellipsoids. Let $s(E_i, E_j)$ denote the similarity between E_i and E_j. There are many definitions of similarity functions in the literature. For our purposes the following properties are used:

$$\text{(s1a)} \quad s(E_i,E_i) = 1 \quad \forall\ i \tag{2a}$$

$$\text{(s1b)} \quad s(E_i,E_j) = 1 \Leftrightarrow E_i = E_j \tag{2b}$$

$$\text{(s2)} \quad s(E_i,E_j) = s(E_j,E_i) \quad \forall\ i \neq j \tag{3}$$

$$\text{(s3)} \quad s(E_i,E_j) > 0 \quad \forall\ i,j \tag{4}$$

Functions that satisfy (2a), (3), and (4) are *weak similarity measures*. Functions that satisfy (2b), (3), and (4) are *strong similarity measures*. Strong similarity measures are also weak, and are simply called similarity measures. Weak similarity measures correspond to pseudometric dissimilarities.

An ellipsoid $E(A, \mathbf{m}; 1)$ is defined by its matrix A and center $\mathbf{m}$. Any ellipsoid can be created by applying a scaling, rotation, and translation of a unit (hyper)sphere. The matrix A scales and rotates the underlying space so that it maps the ellipse into a unit sphere (hence, $\|\mathbf{x}-\mathbf{m}\|_A^2 = 1$for every point $\mathbf{x}$ on the surface of the ellipsoid). Scaling a spheroid is done by matrix multiplication with a scaling matrix S,

$$S = \begin{bmatrix} s_1 & 0 & \cdots & 0 \\ 0 & s_2 & \cdots & 0 \\ 0 & \cdots & \ddots & \vdots \\ 0 & \cdots & 0 & s_p \end{bmatrix} \tag{5}$$

where s_k is the scaling factor for dimension k, $1 \le k \le p$. Rotation through an angle θ is accomplished by matrix multiplication with a unitary rotation matrix R ($R^T = -R^{-1}$), which in $p=2$ space has the form

$$R = \begin{bmatrix} \cos\theta & -\sin\theta \\ \sin\theta & \cos\theta \end{bmatrix} \tag{6}$$

Any point $\mathbf{z}$ in the unit sphere can be mapped to an ellipsoid via scaling, rotation, and shift:

$$\mathbf{z} \to \mathbf{x} = RS\mathbf{z} + \mathbf{m}, \quad \|\mathbf{z}\|_A^2 \le 1 \tag{7}$$

Now we are ready to discuss measures of similarity on pairs of ellipsoids. We begin with a measure that combines the three elements of similarity for geometric structures of this type.

3. Compound similarity

We use subscripts 1 and 2 for a pair of ellipsoids. Our first measure of similarity is a compound measure, the product of three exponential factors that satisfies requirements (2a), (2b), (3), and (4) for strong similarity. This measure of similarity is built by considering the location, orientation, and shape of an ellipse. The geometric rationale and limit behavior of each factor are discussed next.

Location: Positional similarity for (E_1, E_2) is a function of their mean separation, i.e., the distance $\|\mathbf{m}_1 - \mathbf{m}_2\|$ between their centers. Use any vector norm on $\Re^p$ to define

$$g_1(E_1,E_2) = e^{-\|\mathbf{m}_1 - \mathbf{m}_2\|} \tag{8}$$

The function g_1 satisfies (3) and (4), and $E_1 = E_2 \Rightarrow e^{-\|\mathbf{m}_1 - \mathbf{m}_2\|} = 1$, but $\mathbf{m}_1 = \mathbf{m}_2$ does *not* imply that $E_1 = E_2$ (see the *left* view of Fig. 3). In the limit, $e^{-\|\mathbf{m}_1 - \mathbf{m}_2\|} \to 0$ as $\|\mathbf{m}_1 - \mathbf{m}_2\| \to \infty$. The center and right views in Fig. 3 illustrate the most common situation for sample-based ellipsoids, viz., that they have different effective radii, orientation, and centers.

Orientation: For $E_1 = (A_1, \mathbf{m}_1, 1)$ and $E_2 = (A_2, \mathbf{m}_2, 1)$ we define the orientation of each ellipse using the rotation matrices R_1 and R_2, the eigenvector matrices of A_1 and A_2. The angle of rotation between the two ellipsoids is found by projecting the basis vectors of R_1 onto the associated basis vectors of R_2, where the association is established by ranking each basis with the ordered eigenvalues of its matrix. The angles are found by calculating the vector of angles between associated eigenvectors as

$$\theta = \arccos(\mathrm{diag}(R_1^T R_2)) \tag{9}$$

Rotational similarity between E_1 and E_2 is assessed by measuring the set of angles between the associated eigenvector pairs. More specifically, let $\sin\boldsymbol{\theta} = (\sin\theta_1, \ldots, \sin\theta_p)^T$ and define

$$g_2(E_1,E_2) = e^{-\|\sin\boldsymbol{\theta}\|} \tag{10}$$

The function g_2 satisfies (3) and (4). When $E_1 = E_2$, their associated eigenvectors are parallel; hence $E_1 = E_2 \Rightarrow e^{-\|\sin\boldsymbol{\theta}\|} = 1$. When the principal vectors are perpendicular, g_2 takes its maximum value, which is $e^{-\|\sin\boldsymbol{\theta}\|} = e^{\sqrt{p}}$ when the norm is Euclidean. But, again, $\boldsymbol{\theta} = 0$ does *not* imply that $E_1 = E_2$ (e.g., see the *left* view of Fig. 3).

The final piece in our similarity puzzle is *shape*. The eigenstructure of A is the key to assessing the shape of $E(A,\mathbf{m};1)$. Invariants of A to rotation and translation that might be useful in comparing the shapes of two ellipsoids include: tr(A) (sum of the eigenvalues = total variance); det(A) (product of the eigenvalues = generalized variance); scatter volume (a function of det(A)); and normalized scatter volume (a "decorrelated" function of det(A)). Each of these functions has some merit, but also a deficiency. For example, let $p=3$ and suppose that {1, 1, 27} and {3, 3, 3} are the eigenvalues for E_1 and E_2. The determinants and scatter volumes for E_1 and E_2 are equal, but E_1 and E_2 have quite different shapes. E_1 is circular in cross section, but very elongated in its principal direction, while E_2 is a sphere. We turn to a different function of the eigenvalues to characterize shape similarity for a pair of ellipsoids.

Let $\boldsymbol{\alpha} = \{\alpha_1 \le \alpha_2 \le \cdots \le \alpha_p\}$ and $\boldsymbol{\beta} = \{\beta_1 \le \beta_2 \le \cdots \le \beta_p\}$ be the ordered eigenvalues of A_1 and A_2, and recall that the semi-axial length of $E_1 = E(A_1, \mathbf{m}_1; 1)$ from $\mathbf{m}_1$ to its surface in the kth direction is $1/\sqrt{\alpha_k}$, and likewise for E_2. If the ellipsoids have the form $E = E(A, \mathbf{m}, t)$, we adjust the eigenvalues to account for the transformation $A/t^2 \leftarrow A$ that normalizes them to the form $E(A, \mathbf{m}, 1)$. Letting $\boldsymbol{\alpha}^* = (1/\sqrt{\alpha_1}, \ldots, 1/\sqrt{\alpha_p})^T$ and $\boldsymbol{\beta}^* = (1/\sqrt{\beta_1}, \ldots, 1/\sqrt{\beta_p})^T$, define, for any vector norm,

$$g_3(E_1,E_2) = e^{-\|\boldsymbol{\alpha}^* - \boldsymbol{\beta}^*\|} \tag{11}$$

Function g_3 satisfies (3) and (4), and $E_1 = E_2 \Rightarrow g_3(E_1,E_2) = 1$, because the (ordered) eigenvalues of the two ellipsoids are equal, but again, the converse is not guaranteed. Switching notation from (1, 2) to (i, j), we define the product of g_1, g_2, and g_3 as the *compound similarity* between the ellipsoid pair (E_i, E_j):

$$\begin{aligned} s_c(E_i,E_j) &= \underbrace{e^{-\|\mathbf{m}_i - \mathbf{m}_j\|}}_{a} \quad \underbrace{e^{-\|\sin\boldsymbol{\theta}\|}}_{b} \quad \underbrace{e^{-\|\boldsymbol{\alpha}^* - \boldsymbol{\beta}^*\|}}_{c} \\ &\quad \text{location} \qquad \text{orientation} \qquad \text{shape} \\ &= e^{-(\|\mathbf{m}_j - \mathbf{m}_j\| + \|\sin\boldsymbol{\theta}\| + \|\boldsymbol{\alpha}^* - \boldsymbol{\beta}^*\|)} \end{aligned} \tag{12}$$

We summarize the properties of $s_c(E_i, E_j)$ in

Proposition 1. *Let $E_i = E(A_i, \mathbf{m}_i; t_i)$ and $E_j = E(A_j, \mathbf{m}_j; t_j)$ be (hyper)-ellipsoids in p-space. Let the eigenvalue–eigenvector pairs for E_i and E_j be $\{0 \le \alpha_1 \le \alpha_2 \le \cdots \le \alpha_p\} \leftrightarrow \{\mathbf{u}_1, \mathbf{u}_2, \ldots, \mathbf{u}_p\}$ and $\{0 \le \beta_1 \le \beta_2 \le \cdots \le \beta_p\} \leftrightarrow \{\mathbf{v}_1, \mathbf{v}_2, \ldots, \mathbf{v}_p\}$. Let $\boldsymbol{\alpha} = (\alpha_1 = \alpha_m, \ldots, \alpha_p = \alpha_M)^T$, $\boldsymbol{\beta} = (\beta_1 = \beta_m, \ldots, \beta_p = \beta_M)^T$, $\boldsymbol{\alpha}^* = (1/\sqrt{\alpha_1}, \ldots, 1/\sqrt{\alpha_p})^T$, and $\boldsymbol{\beta}^* = (1/\sqrt{\beta_1}, \ldots, 1/\sqrt{\beta_p})$. Define $\boldsymbol{\theta}$ as the angle between eigenvector pairs $\mathbf{u}_i$ and $\mathbf{v}_i$, $1 \le i \le p$. Then*

(s1) $s_c(E_i,E_j) = 1 \Leftrightarrow E_i = E_j$ (13)

(s2) $s_c(E_i,E_j) = s(E_j,E_i) \quad \forall\ i \ne j$ (14)

(s3) $s_c(E_i,E_j) > 0 \quad \forall\ i,j$ (15)

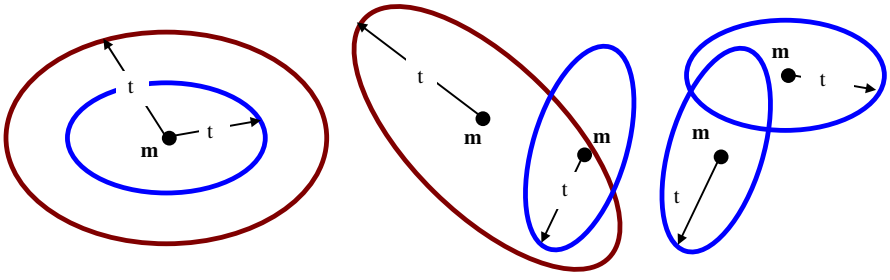

Fig. 3. Different effective radii and centers for two ellipsoids.

Proof. First suppose that $E_i=E_j$. Then $(\mathbf{m}_i=\mathbf{m}_j)$, $\theta_{u_i v_i}=0^\circ$ $\forall\ i\Rightarrow\theta=\mathbf{0}$, and $\widehat{\boldsymbol{\alpha}}=\widehat{\boldsymbol{\beta}}$. Thus, the argument of each exponential factor in (12) is 0, and hence, $s_c(E_i, E_j)=1$. Now assume that $s(E_i, E_j)=1$. We know that each individual factor in (12) can be 1, and yet, $E_i\neq E_j$. However, taking the factors jointly as a product will insure that $E_i=E_j$. To see this, view (12) as the product of the 3 positive numbers a, b, and c, so $s_c(E_i, E_j)=abc=1$. We show that all three factors are 1 by contradiction. Suppose, to the contrary, that there is a pair of reciprocals, say a and $b=1/a$, such that $ab=1$ and neither a nor b is 1. The factors a, b, and c are valued in (0, 1], so if $b\neq 1$, then $b<1$. From this it follows that $a=1/b>1$. This contradicts the fact that $a\in(0,1]$. The same argument holds for any pair of factors, so we conclude that when the product at (12) is 1, $a=b=c=1$.

To complete the proof, equate each factor in (12) to 1. For example, $e^{-\|\mathbf{m}_i-\mathbf{m}_j\|}=1\ \Leftrightarrow\|\mathbf{m}_i-\mathbf{m}_j\|=0\Leftrightarrow\mathbf{m}_i=\mathbf{m}_j$, which shows that E_i and E_j have the same means. Similar arguments show that these two ellipsoids also have equal orientations, and equal eigenstructures (shapes). Thus, while any one of the three factors being 1 does not guarantee that $E_i=E_j$, when all three factors take the value 1, E_i must equal E_j. This proves (13). We finish the proof by noting that properties (14) and (15) are true, since each factor is symmetric and valued in (0, 1]. □

Proposition 1 shows that s_c is a similarity measure on pairs of (hyper)ellipsoids. However, we discovered during initial experiments using this measure with the Euclidean norm in the exponent that it was quite sensitive to small changes in the location of the mean (center) of E_i and/or E_j. Using a statistical distance for normalization of s_c reduces this problem. Accordingly, the measure of similarity we will study is

$$s_{cn}(E_i,E_j)=e^{-\left(\|\mathbf{m}_i-\mathbf{m}_j\|^2_{(A_i+A_j)^{-1}}+\|\sin\boldsymbol{\theta}\|+\|\boldsymbol{\alpha}^*-\boldsymbol{\beta}^*\|\right)} \tag{16}$$

where the measure of distance between $\mathbf{m}_i$ and $\mathbf{m}_j$ is the Mahalonobis distance induced by the pooled (covariance) matrices of E_1 and E_2, viz., $\|\mathbf{m}_i-\mathbf{m}_j\|^2_{(A_i+A_j)^{-1}}=(\mathbf{m}_i-\mathbf{m}_j)^T(A_i+A_j)^{-1}(\mathbf{m}_i-\mathbf{m}_j)$. This change does not alter the proof of Proposition 1, so s_{cn} is a *compound*, *normalized* similarity measure.

4. Transformation energy similarity

Consider each ellipsoid as having its own space spanned by its eigenvector basis with origin at its center. We can construct a function that maps a point from one ellipsoid space to another via the common space between them. A point in the space of ellipsoid E_i can be mapped to the common co-ordinate space by scaling the point by S_i^{-1}, reversing the rotation by R_i^{-1}, then shifting the point away from the origin by translation by $\mathbf{m}_i$. Within this common space the point can then be mapped into the space of E_j by shifting the point by $\mathbf{m}_j$, rotating by R_j and scaling by S_j. The mapping is summarized as

$$\mathbf{x}_j=f(\mathbf{x}_i|E_i,E_j)=S_jR_j(R_i^{-1}S_i^{-1}\mathbf{x}_i-\mathbf{m}_i+\mathbf{m}_j)$$

$$=\underbrace{S_jR_jR_i^{-1}S_i^{-1}}_{M_{ij}}\mathbf{x}_i+\underbrace{S_jR_j(\mathbf{m}_j-\mathbf{m}_i)}_{\mathbf{d}_{ij}}=M_{ij}\mathbf{x}_i+\mathbf{d}_{ij} \tag{17}$$

where $E_i=E(R_iS_i^{-2}R_i^T,\mathbf{m}_i;1)$, $E_j=E(R_jS_j^{-2}R_j^T,\mathbf{m}_j;1)$. The norm of this function is a measure of the "amount of energy expended" to make the transformation,

$$\|f(E_i,E_j)\|_2=\underbrace{\max_{\substack{\mathbf{z}\in\Re^p\\ \|\mathbf{z}\|_2=1}}}\ \{\|f(\mathbf{z}|(E_i,E_j)\|_2\} \tag{18}$$

Since (18) is not necessarily symmetric in the arguments of f, $\|f(E_i,E_j)\|_2\neq\|f(E_j,E_i)\|_2$, we account for asymmetry by utilizing the norms in both directions. Thus, we define the *transformation energy* similarity function as

$$s_{te}(E_i,E_j)=1\Big/\underbrace{\max_{\substack{\mathbf{z}\in\Re^p\\ \|\mathbf{z}\|_2=1}}}\ \{(\|f(E_i,E_j)\|_2,\|f(E_j,E_i)\|_2)\} \tag{19}$$

Proposition 2. *$s_{te}(E_i, E_j)$ is a similarity function satisfying Eqs.* (2), (3), and (4).

Proof. We begin the proof by stating and proving two results that concern the *spectral norm* $\|A\|_2$ of a matrix A. □

Lemma 1. *If A is any invertible matrix, then* $\max\{\|A\|_2,\|A^{-1}\|_2\}\geq 1$.

Proof. A is invertible, so its singular values are all positive. Let $0<\sigma_1\leq\sigma_2\leq\cdots\leq\sigma_t$ be the singular values of A, so $0<1/\sigma_t\leq 1/\sigma_{t-1}\leq\cdots\leq 1/\sigma_1$ are the singular values of A^{-1}. The spectral norm of A is its largest singular value, so $\max\{\|A\|_2,\|A^{-1}\|_2\}=\max\{\sigma_t,1/\sigma_1\}$. Either $\sigma_t\geq 1\Rightarrow\max\{\sigma_t,1/\sigma_1\}\geq 1$, or $\sigma_t<1\Rightarrow 1/\sigma_1>1\Rightarrow\max\{\sigma_t,1/\sigma_1\}>1$. □

Lemma 2. *If A and B are invertible matrices and* $\max\{\|B^{-1}A\|_2,\|A^{-1}B\|_2\}=1\Rightarrow A^{-1}B=(B^{-1}A)^T$.

Proof. Let $X=A^{-1}B$ have singular values $0<\sigma_1\leq\sigma_2\leq\cdots\leq\sigma_t$, so $X^{-1}=B^{-1}A$ has singular values $0<1/\sigma_t\leq 1/\sigma_{t-1}\leq\cdots\leq 1/\sigma_1$. If $\sigma_t=\|X\|_2=1\Rightarrow\sigma_1\leq 1\Rightarrow 1/\sigma_1=\|X^{-1}\|_2\geq 1$. Suppose that $\sigma_t=\|X\|_2=1$. Then $\sigma_1\leq 1\Rightarrow 1/\sigma_1=\|X^{-1}\|_2\geq 1$. If $1/\sigma_1>1$, then $\max\{\|B^{-1}A\|_2,\|A^{-1}B\|_2\}>1$, which contradicts the hypothesis. Thus $\sigma_1=1\Rightarrow\sigma_k=1\ \forall\ k$, and we have the identity matrix I for the diagonal part of the singular value decomposition of X, i.e., $X=U[I]V^T=UV^T=$ where U and V are unitary. Thus $X^TX=XX^T=I$ and $X^{-1}=X^T$. □

Now suppose that $E_i=E_j$, the scaling and rotation matrices and ellipsoid centers are equal, $S_i=S_j$, $R_i=R_j$ and $\mathbf{m}_i=\mathbf{m}_j$, $M_{ij}=I_p$ is the $p\times p$ identity matrix, $\mathbf{d}_{ij}=\mathbf{0}$, and so $s_{te}(E_i, E_j)=1$. Conversely, it is not obvious that $s_{te}(E_i, E_j)=1\Rightarrow E_i=E_j$. Lemma 1 yields $s_{te}(E_i,E_j)=1/\max\{(\|f(E_i,E_j)\|_2,\|f(E_j,E_i)\|_2)\}=1/\max\left\{\left(\|M_{ij}\|_2,\|M_{ij}^{-1}\|_2\right)\right\}\leq 1$. Thus, $s_{te}(E_i,E_j)=1\Rightarrow s_{te}(E_i,E_j)=1/\max\{\|f_1(E_i,E_j)\|_2,\|f_1(E_j,E_i)\|_2\}$ and hence $\mathbf{m}_i=\mathbf{m}_j$. From this we can also deduce that $0\leq s_{te}(E_i, E_j)\leq 1$, and hence, $s_{te}(E_i,E_j)=1\Leftrightarrow\max\{\|f_1(E_i,E_j)\|_2,\|f_1(E_j,E_i)\|_2\}=1$ Finally, this implies $E_i=E_j$ by applying Lemma 2 to $f_1(E_i,E_j)=\|S_jR_jR_i^{-1}S_i^{-1}\|_2$ which yields $(S_jR_jR_i^{-1}S_i^{-1})^T S^jR^jR_i^{-1}S_i^{-1}=I$, whence

$$(S_i^{-1})^T(R_i^{-1})^TR_j^TS_j^TS_jR_jR_i^{-1}S_i^{-1}=I. \tag{20}$$

We know that S_i and S_j are diagonal, and R_i and R_j are unitary, so we have two cases. If $S_j=I$, Eq. (20) simplifies to $(S_i^{-1})^TS_i^{-1}=I\Rightarrow S_i=I$. If $S_j\neq I$, we must have $S_j^{-1}=R_jR_i^{-1}S_i^{-1}$ in order for Eq. (20) to hold. This implies that $S_j=S_i$ and $R_j=R_i$. Therefore, if $s(E_i, E_j)=1$, then either: $S_i=S_j=I$ and $\mathbf{m}_i=\mathbf{m}_j$, implying that E_i and E_j are spheres, which are not affected by rotation, so $E_i=E_j$; or $S_i=S_j$, $R_i=R_j$, $\mathbf{m}_i=\mathbf{m}_j$, so that again, $E_i=E_j$. To complete the proof, we see from (19) that $s_{te}(E_i, E_j)=s_{te}(E_j, E_i)$ for all $i\neq j$, and since this similarity function is the inverse of a norm, $s_{te}(E_i, E_j)\geq 0$ for all $i\neq j$. □

Remark. If (18) must be solved many times, this problem can become computationally expensive. When the number of comparisons needed is large, we can replace (19) by an approximation to $s_{te}(E_i, E_j)$, which avoids this difficulty by observing that $\|g_1\|_2\leq\|g_1+g_2\|_2\leq\|g_1\|_2+\|g_2\|_2$. This suggests taking $\|f(E_i,E_j)\|_2\approx\|f_1(E_i,E_j)\|_2+\|f_2(E_i,E_j)\|_2$, where $f_1(E_i,E_j)=M_{ij}\mathbf{x}_i$ and $f_2(E_i,E_j)=d_{ij}$ as

in (17). The value of each term in this approximation is given by the largest singular value of M_{ij}, $\|f_1(E_i,E_j)\| = \|M_{ij}\mathbf{x}_i\| = \sigma_{ij,1}$ and likewise for the second term. Using the Euclidean norm for $\mathbf{d}_{ij}$ then gives

$$s_{t\tilde{e}}(E_i,E_j) = 1/\max\{(\sigma_{ij,1}+\|\mathbf{d}_{ij}\|_2, \sigma_{ji,1}+\|\mathbf{d}_{ji}\|_2)\} \le s_{te}(E_i,E_j) \le 1/\max\{\sigma_{ij,1},\sigma_{ji,1}\} \quad (21)$$

with equality when $\|\mathbf{d}_{ij}\|_2 = \|\mathbf{d}_{ji}\|_2$, or, equivalently, $\mathbf{m}_i = \mathbf{m}_j$.

The approximation function $s_{t\tilde{e}}(E_i,E_j)$ satisfies requirements (3) and (4), and it is clear that when $E_i = E_j$ $s_{t\tilde{e}}(E_i,E_j) = 1$. However, $s_{te}(E_i, E_j)$ is an *upper bound* on $s_{t\tilde{e}}(E_i,E_j)$, so $s_{te}(E_i, E_j) = 1$ does not guarantee that $s_{t\tilde{e}}(E_i,E_j) = 1$. We do not have an estimate for the tightness of this upper bound, but we did compute this approximation in all of our numerical experiments as a check on the exact value, and, in most cases, the approximation is pretty close to its upper bound. So, when n is large, the approximation $s_{te} \approx s_{t\tilde{e}}$ is a good alternative to using (19) directly.

5. Focal similarity

Our third measure of similarity begins by recalling that every plane ellipse can be constructed by tracing the curve whose distance from a pair of foci $\mathbf{f}_1$ and $\mathbf{f}_2$ is some positive constant $c(t)$, which depends on the effective radius t.

This construction is shown for a two-dimensional ellipse in Fig. 4, with effective radius t so that $p(t)+q(t)=c(t)$ for the ellipse $E(A,\mathbf{m}; t)$. The foci always lie along the major axis of the ellipse, which is the linear span of the eigenvector of A corresponding to the maximum eigenvalue. We denote the line segment with endpoints $\mathbf{f}_1$ and $\mathbf{f}_2$ by f_{12}, and call this the *focal segment* of $E(A,\mathbf{m}; t)$.

If $\{\alpha_m \le \alpha_M\}$ are the minimum and maximum eigenvalues of A with corresponding orthogonal eigenvectors $\{\mathbf{u}_\mathbf{m},\mathbf{u}_\mathbf{M}\}$, the locations of the foci are $\mathbf{f}_{1,2} = \mathbf{m} \pm \frac{1}{2}\sqrt{((\alpha_M-\alpha_m)/\alpha_M\alpha_m)}\mathbf{u}_\mathbf{M}$. The *focal similarity* between E_1 and E_2 is defined as the average of a set of four distances. Each component is defined by a distance to one of the focal segments e_{12} or f_{12}.

Let $d(\mathbf{x},\mathbf{y}) = \|\mathbf{x}-\mathbf{y}\|$ be the Euclidean distance between vectors in $\mathbf{x},\mathbf{y} \in \Re^p$. We have two focal segments, e_{12} with endpoints $\mathbf{e}_1$ and $\mathbf{e}_2$, and f_{12} with endpoints $\mathbf{f}_1$ and $\mathbf{f}_2$. We compute four default distances:

$$\delta_1 = \min\{d(\mathbf{e}_1,\mathbf{f}_1), d(\mathbf{e}_1,\mathbf{f}_2)\} \quad (22)$$

$$\delta_2 = \min\{d(\mathbf{e}_2,\mathbf{f}_1), d(\mathbf{e}_2,\mathbf{f}_2)\} \quad (23)$$

$$\delta_3 = \min\{d(\mathbf{f}_1,\mathbf{e}_1), d(\mathbf{f}_1,\mathbf{e}_2)\} \quad (24)$$

$$\delta_4 = \min\{d(\mathbf{f}_2,\mathbf{e}_1), d(\mathbf{f}_2,\mathbf{e}_2)\} \quad (24)$$

One or more of the values in (22)–(25) may be replaced using the following heuristic. For each foci "**f**", if the orthogonal projection of "**f**" to the linear span of the opposing maximal eigenvector falls on the opposing focal segment then we replace the appropriate default distance by this distance; otherwise we find the minimum distance between "**f**" and the two opposing foci and use it in one of the Eqs. (22)–(25). In other words, if the orthogonal projection does not fall on the opposing focal segment it will not be considered in the calculation. We now define the

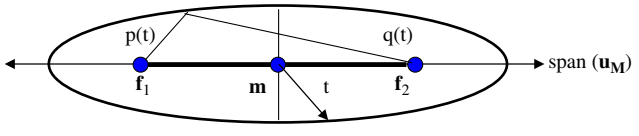

Fig. 4. Focal points $\mathbf{f}_1$ and $\mathbf{f}_2$ and focal segment f_{12} of $E(A, \mathbf{m}; t)$.

focal distance between the ellipsoids E_1 and E_2 as the average of these four distances:

$$d_{fd}(E_1,E_2) = \mathrm{dis}(e_{12},f_{12}) = \frac{\delta_1+\delta_2+\delta_3+\delta_4}{4} \quad (25)$$

Now let $E_1(A_1, \mathbf{m}_1; t_1)$ and $E_2(A_2, \mathbf{m}_2; t_2)$ be non-degenerate ellipsoids in $\Re^p$. Let $\boldsymbol{\alpha}=\{\alpha_1 \le \alpha_2 \le \cdots \le \alpha_p\}$ and $\boldsymbol{\beta}=\{\beta_1 \le \beta_2 \le \cdots \le \beta_p\}$ be the eigenvalues of A_1 and A_2. Adjust the eigenvalues to $\boldsymbol{\alpha}^* = (1/\sqrt{\alpha_1},\ldots,1/\sqrt{\alpha_p})^T$ and $\boldsymbol{\beta}^* = (1/\sqrt{\beta_1},\ldots,1/\sqrt{\beta_p})^T$. There are $p(p-1)/2$ focal segments for the two-dimensional ellipses spanned by each pair of eigenvectors of E_1 and E_2. Thus, there are $(p-1)$ "ordered" focal distances between pairs of focal segments of the two ellipsoids. We define the *generalized focal distance* between E_1 and E_2 as the average of the plane focal distances:

$$d_{gfd}(E_1,E_2) = \frac{\sum_{j=1}^{p-1} \mathrm{dis}(e_{j,j+1},f_{j,j+1})}{(p-1)} \quad (26)$$

Note that when $p=2$, (26) reduces to (25). The generalized focal distance d_{gfd} is *almost* a metric on pairs of ellipsoids. We say almost because for the simplest case, $p=2$, it can happen that $d_{fd}(E_1, E_2)=0$ but $E_1 \ne E_2$. Recall that a *pseudometric* on a set X is a non-negative real-valued function $d : X \times X \mapsto [0,\infty)$ such that, for x, y, z in X,

pm1. $d(x, x)=0$
pm2. $d(x, y)=d(y, x)$ (symmetry)
pm3. $d(x, z) \le d(x, y)+d(y, z)$ (subadditivity/triangle inequality)

Proposition 3. *d_{fd} in* (25) *is a* pseudometric *on pairs of p-dimensional ellipsoids.*

Proof. Since each of the four factors in (25) is a metric, their average is symmetric, and it is easy to check that it also satisfies the triangle inequality, so pm2 and pm3 hold. Since each factor of (25) is a metric, pm1 holds for any ellipse, $d_{fd}(E_1, E_1)=0$. To see that d_{fd} is not positive definite, consider the construction of an ellipse E_1 as shown in Fig. 4, where, for $t=t_1$, $p(t_1)+q(t_1)=c(t_1)$. Now construct a second ellipse E_2 with the same focal segment but a different radius t_2, so that for E_2, $p(t_2)+q(t_2)=c(t_2)$. This pair of ellipses has the same focal segment, so $d_{fd}(E_1, E_2)=0$, but since $c(t_1) \ne c(t_2)$, $E_1 \ne E_2$. Hence, d_{fd} is a pseudometric. □

Corollary 1. *Let D_{fd} be a collection of n^2 normalized values of d_{fd} in* (25) *on n ellipsoids,* say $[D_{fd,ij}]=[d_{fd}(E_i, E_j)/\max_{(s,t,\ s\ne t)}\{d_{fd}(E_s, E_t)\}]$. *Define $s_{fs}=1-d_{fd}$. Since d_{fd} is a pseudometric, $s_{fs}(E_i, E_j)$ satisfies Eqs.* (3) *and* (4). *In view of Proposition* 3, *we know that $s_{fs}(E_s, E_t)=1$ does not imply that $E_s=E_t$, so s_{fs} is not a strong similarity measure. But s_{fs} satisfies* (2a), *so it is a weak similarity measure. We call s_{fs} the* focal similarity *between E_i and E_j.*

Since the generalized focal distance is the average of $(p-1)$ focal distances that all satisfy Corollary 1, the generalized focal distance also satisfies the statement made in Corollary 1.

Corollary 2. *Let D_{gfd} be a collection of n^2 normalized values of d_{fd} in* (25) *on n ellipsoids, say* $[D_{gfd,ij}]=[d_{gfd}(E_i, E_j)/\max_{(s,t,\ s\ne t)}\{d_{gfd}(E_s, E_t)\}]$. *Define $s_{gfs}=1-d_{gfd}$. Since d_{gfd} is a pseudometric, $s_{gfs}(E_i, E_j)$ satisfies Eqs.* (3) *and* (4). *In view of Proposition* 3, *we know that $s_{gfs}(E_s, E_t)=1$ does not imply that $E_s=E_t$, so s_{gfs} is not a strong similarity measure. But s_{gfs} does satisfy* (2a), *so it is a weak similarity measure. We call s_{gfs} the* generalized focal similarity *between E_i and E_j.*

Fig. 5 depicts a few cases for the four distances comprising (25), where for ease of interpretation, we show focal segments and

distances without notation. The solid green lines represent endpoint distances, and the double red lines are distances of orthogonal projections that land on opposing focal segments (so red lines may represent "replacement distances" for each of (22)–(25)).

Fig. 5(a) has four equal distances (or put another way, one distinct distance); (b) and (c) have two distinct distances; (d) and (e) have three distinct distances; and (f) has four distinct distances. There are other cases, but these suffice to explain the concept. While (25) appears to be quite different from the first two similarity measures, the focal distance does account for location, shape, and orientation.

Example 1. To conclude this section we compare s_{cn}, s_{te} and s_{fs} with five simple examples. Normalization of E_i and E_j via $A_i/t_i^2 \leftarrow A_i$ and $A_j/t_j^2 \leftarrow A_j$ is always done for synthetically generated ellipsoids. For sample-based ellipsoids, t is not known, but is not needed for a complete analysis. We used Matlab's constrained nonlinear optimization, fmincon, which is a Trust-Region Reflective Algorithm discussed in [36], when computing the transformation energy similarity function at (18).

Table 1 contains five pairs of ellipses, and shows beneath them the value of each similarity coefficient for each pair. Look at these five examples, decide for yourself, which pairs of ellipsoids are "most different" and "most similar", and then compare your assessment to the ones rendered by the numerical indices, whose maximums and minimums are highlighted in boldface type.

Fig. 6 plots the values of the three coefficients for cases A–E shown in Table 1. On the horizontal axis the ticked labels are $A=1$, $B=2$, $C=3$, $D=4$, $E=5$. All three measures agree that case D exhibits the least similar pair, and most observers would agree with this assessment. But while the three indices all agree that case E is the most similar pair, our guess is that most observers would disagree with this result, and instead choose pair C as the most similar. We think the explanation for the apparent discrepancy between human observation and mathematical assessment lies with the properties of the ellipses. Case E features two ellipses with the same means, but different shapes and orientations, while Case C has a pair of ellipses with the same shape and orientation, but different means. This suggests that the three models weight central tendency more heavily than humans do. The important point is that all three measures agree—here. But we shall see below that they are quite different on more complex sets of ellipses.

There may be (perhaps often will be) many ellipse pairs, which have very nearly the same or even equal similarity values that have very different spatial configurations using any of these measures, even when $p=2$. (We know this to be the case for the focal similarity.) To see that it can also happen for the other measures, consider $s_{cn}=abc$, the product of three numbers a, b, and c all of which lie in [0,1]. Suppose $s_{cn}=0.5$ and $a=1$. Then (bc) must equal 0.5 with b and c in (0,1], but are otherwise unconstrained, so there are many ellipse pairs – all different from one another – that result in this single value. While this observation seems to deflate the value of measuring similarity by any of these functions, in practice we will rarely, if ever, encounter a "tie", wherein two quite different ellipse pairs yield the same value of any of these measures.

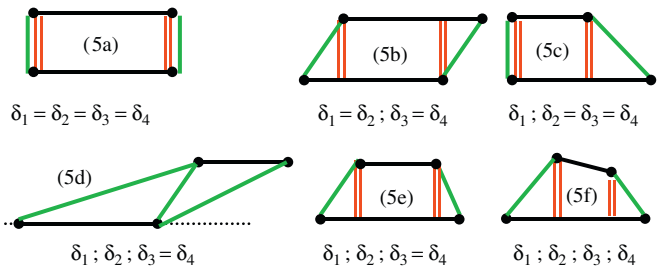

Fig. 5. Several cases of different focal distance components of d_{fd} at (25).

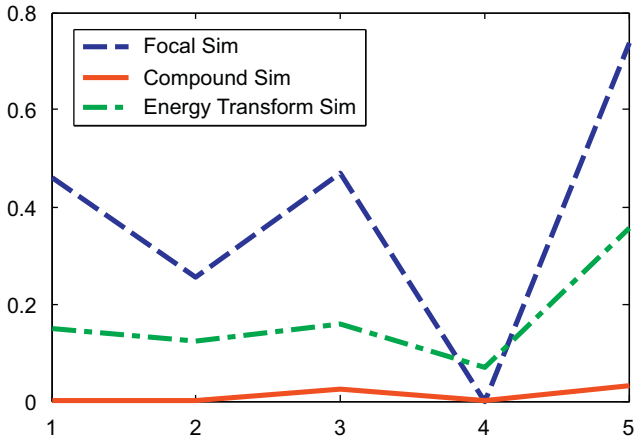

Fig. 6. Similarity coefficients for the five ellipse pairs in Table 1.

Table 1
Some examples of ellipsoidal similarity.

A	B	C	D	E
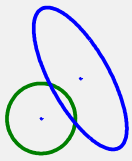	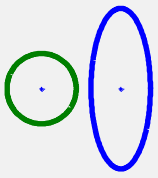	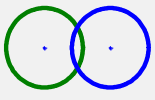	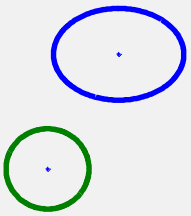	
$s_{cn}(E_i, E_j)=0.018$ $s_{te}(E_i, E_j)=0.148$ $s_{fs}(E_i, E_j)=0.460$	$s_{cn}(E_i, E_j)=0.001$ $s_{te}(E_i, E_j)=0.122$ $s_{fs}(E_i, E_j)=0.225$	$s_{cn}(E_i, E_j)=0.024$ $s_{te}(E_i, E_j)=0.16$ $s_{fs}(E_i, E_j)=0.469$	$s_{cn}(E_i, E_j)=0.000$ $s_{te}(E_i, E_j)=0.07$ $s_{fs}(E_i, E_j)=0.00$	$s_{cn}(E_i, E_j)=0.031$ $s_{te}(E_i, E_j)=0.355$ $s_{fs}(E_i, E_j)=0.737$

6. Tendency assessment with VAT and iVAT

Our aim is to use similarity and dissimilarity measures and their iVAT images to find clusters in sets of ellipsoids. Before considering this specific problem, we introduce some concepts from clustering theory that are needed to proceed with our objectives. Clustering is the problem of partitioning a set of unlabeled objects $O=\{o_1, \ldots, o_n\}$ into groups of similar objects [1,7,16–20]. The field comprises three *canonical problems* (CPs). (CP1) is *assessment*: prior to finding any clusters, we ask—*are there* clusters in O; if so, how many? (CP2) is *clustering*: *what are* the clusters in O? (CP3) is *validation:* are the found clusters "*good*" in any useful or meaningful way? When $o_i \in O$ is represented by $\mathbf{x}_i \in \Re^p$, $X=\{\mathbf{x}_1, \ldots, \mathbf{x}_n\}$ is an *object data* representation of O. The kth component of $\mathbf{x}_i$ is the kth *feature* (e.g., height, hair color, number of legs, etc.) of o_i. When relational values between *pairs* of objects are available, we have *relational data*. Any relation ρ on $O \times O$ is representable by a square matrix $R_{n\times n}=[r_{ij}]$, where $r_{ij}=\rho(o_i,o_j)$ is the relationship between o_i and o_j, $1 \le i, j \le n$. X can be converted into *dissimilarity* data $D_{n\times n}=[d_{ij}]=[\|\mathbf{x}_i-\mathbf{x}_j\|]$ using any norm on $\Re^p$. Similarity data $S_{n\times n}$ are always convertible to dissimilarity data D using simple transformations such as $D=[1]-S$. This is the method we use for our examples; see [21] for other methods.

Our approach to clustering ellipsoids is based on visual assessment. Visual methods vary greatly in complexity and computational cost from simple techniques such as histograms and box-and-whisker plots to those implemented in larger interactive software systems such as the IBM Open Visualization Data Explorer™ (http://www.research.ibm.com/dx/). A classic reference for the principles of effective visual display is [22]. Many useful data mining and visualization methods are covered in [23,24] is a nice reference for the practical application of some of the known techniques, and [25] contains some classic approaches for visual analysis in multidimensional object vector data.

The visual representation of structure in unlabeled dissimilarity data has a long history. Tryon [26] paved the way for this branch of clustering when he introduced visual assessment and aggregation of hand-rendered profile graphs for all three problems in 1939. Cattell [27] first depicted clusters in pairwise dissimilarity data about the objects in O as an $n \times n$ image. Important advances in visual clustering include Sneath [28], Floodgate and Hayes [29], Ling [30], and the VAT/sVAT/coVAT/iVAT papers [31–35]. The common denominator in all these methods is the *reordered dissimilarity image* (RDI). The intensity of each pixel in an RDI corresponds to the dissimilarity between the addressed row and column objects. An RDI is "useful" if it highlights potential clusters as a set of "dark blocks" along its diagonal. Each dark block represents a group of objects that are fairly similar. We use recursive iVAT to produce RDIs in the sequel.

VAT [31] reorders an input dissimilarity matrix $D \to D^*$ and displays a grayscale image $I(D^*)$ whose ijth element is a scaled dissimilarity value between objects o_i and o_j. Each element on the diagonal of the VAT image is zero. Off the diagonal, the values range from 0 to 1. If an object is a member of a cluster, then it also should be part of a submatrix of "small" values, whose diagonal is superimposed on the diagonal of the image matrix. The iVAT method [34] transforms $D \to D'$ using a path-based distance and then VAT is applied to D' to get D'^*, resulting in an iVAT image $I(D'^*)$.

Constructing the iVAT matrix D' matrix as in [34] can be computationally expensive ($O(n^3)$). The recursive computation of D'^* given here and in [35] does not alter the VAT order of D^* and is $O(n^2)$. Recursive iVAT [35] builds the matrix D'^* more efficiently than iVAT by first applying VAT to $(D) \to D^*$, and then recursively using D^* to build D'^*. The main limitation of iVAT is size; hardware and software limits $D_{n\times n}$ to about $n \approx \mathbf{O}(1\,0^4)$, but for our application, VAT is well within its working capacities. In general, the functions arg max and arg min, in Steps 1 and 2, are set valued, and when the sets contain more than one pair of optimal arguments, any optimal pair can be selected. The result of applying VAT to $D_{n\times n}$ is $D^*_{n\times n}$; and the displayed output is the VAT image $I(D^*_{n\times n})$. The VAT reordering for D^* is stored in array $P=(P(1), \ldots, P(N))$.

VAT/recursive iVAT: visual assessment of tendency [31,34,35]

Input: Dissimilarities $D_{n\times n}$ for $O=\{o_1, \ldots, o_n\}$; (convert similarity data $S_{n\times n}$ as $D=[1]-S$).

Step 1: $K=\{1, \ldots, n\}$; select $(i,j) \in \arg\max_{p\in K, q\in K}\{D_{pq}\}$; set $P(1)=i$; $I=\{i\}$; and $J=K-\{i\}$.

Step 2: For $t=2, \ldots, n$: select $(i,j) \in \arg\min_{p\in I, q\in J}\{D_{pq}\}$; $P(t)=j$; $I \leftarrow I \cup \{j\}$ and $J \leftarrow J-\{j\}$.

Step 3: Form the ordered dissimilarity matrices

[VAT]: D^*: $d^*_{ij}=d_{P(i)P(j)}$ for $1 \le i, j \le n$.

[iVAT]: $D'^*=[0]_{n\times n}$ for $r=2; \ldots; n$ **do**

$$j=\underbrace{\arg\min}_{k=1,\ldots,r-1}\{D^*_{rk}\}$$
$$D'^*_{rc}=D^*_{rc}, \quad c=j$$
$$D'^*_{rc}=\max\{D^*_{rj}, D'^*_{jc}\}, \quad c=1,\ldots,r-1, \quad c \ne j$$

For $2 \le j \le n; i<j: D'^*_{ji}=D'^*_{ij}$

Step 4: Display $I(D^*)$ and $I(D'^*)$, scaled so that $\max_{1\le i,j\le n}\{d^*_{ij}\}$, $\max_{1\le i,j\le n}\{d'^*_{ij}\}$ = white and 0 = black.

Fig. 7(a) is a scatterplot of a "boxes and stripe" data set similar to that used in [34,35]. This two-dimensional data has two round clusters, two rectangular clusters, and one elongated curvilinear cluster. Most would agree that there are $c=5$ clusters in this data. These object data were converted to $D=[d_{ij}]=[\|\mathbf{x}_i-\mathbf{x}_j\|]$ using the Euclidean norm.

The $c=5$ visually apparent clusters in Fig. 7(c) are quite clearly suggested by the 5 distinct dark diagonal blocks in Fig. 7(c), $I(D'^*)$, which is the iVAT RDI of the data. Compare this to view (b), which is the VAT image $I(D^*)$ of these data. $I(D^*)$ presents some evidence supporting the view that this data contains four clusters (the four clouds are seen in both (b) and (c)), but it misses the stripe cluster. Interpretation of substructure in the data suggested by $I(D'^*)$ is a significant improvement. Next we turn to the use of iVAT for assessment of clusters in sets of ellipsoids.

7. Tendency assessment for sets of ellipsoids

Let E denote n ellipsoids in p-space, $E=\{E_1, E_2, \ldots, E_n\}$. For $(E_i, E_j) \in E \times E$, compute $s_{*,ij}=s(E_i, E_j)$ with any of our three measures of similarity, and array these n^2 values as the $n \times n$ similarity relation matrix $S_*=[s_{*,ij}]$. The transformation $D_*=[d_{*,ij}]=[1-s_{*,ij}]$ yields a dissimilarity relation on $E \times E$. (Actually, we need not do this for the focal measure, as it is, by definition, a dissimilarity measure already.) Applying the iVAT algorithm to D_* will yield an RDI that can be used to assess clustering tendencies of the ellipsoids in $E \times E$. We illustrate the use of iVAT images for this purpose with three data sets: $E30$, $E40$, and $E54$. The first two data sets are synthetic (i.e., we constructed these sets of ellipses to form the clusters they appear to have). E54 is the real IBRL data set shown in Fig. 2. The synthetic ellipses are generated with $t=1$, so normalization is not needed, and the sample-based ellipses cannot be normalized because t is unknown.

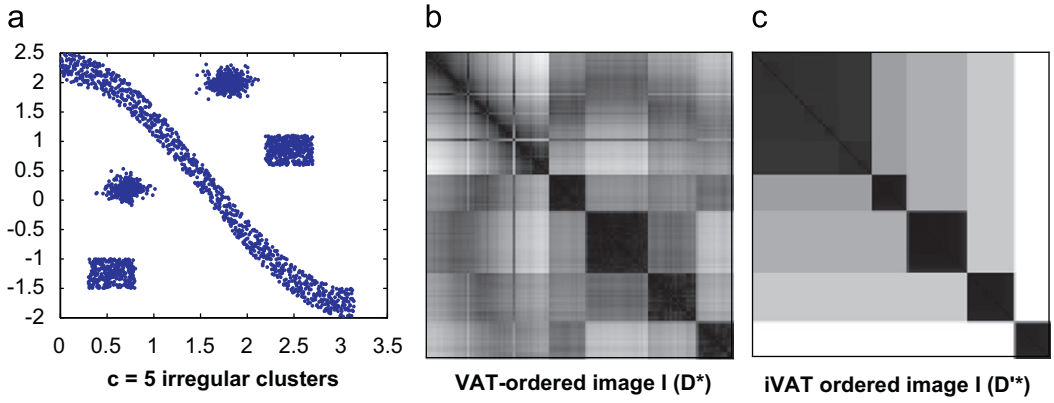

Fig. 7. The VAT and iVAT RDIs of the data in view (a).

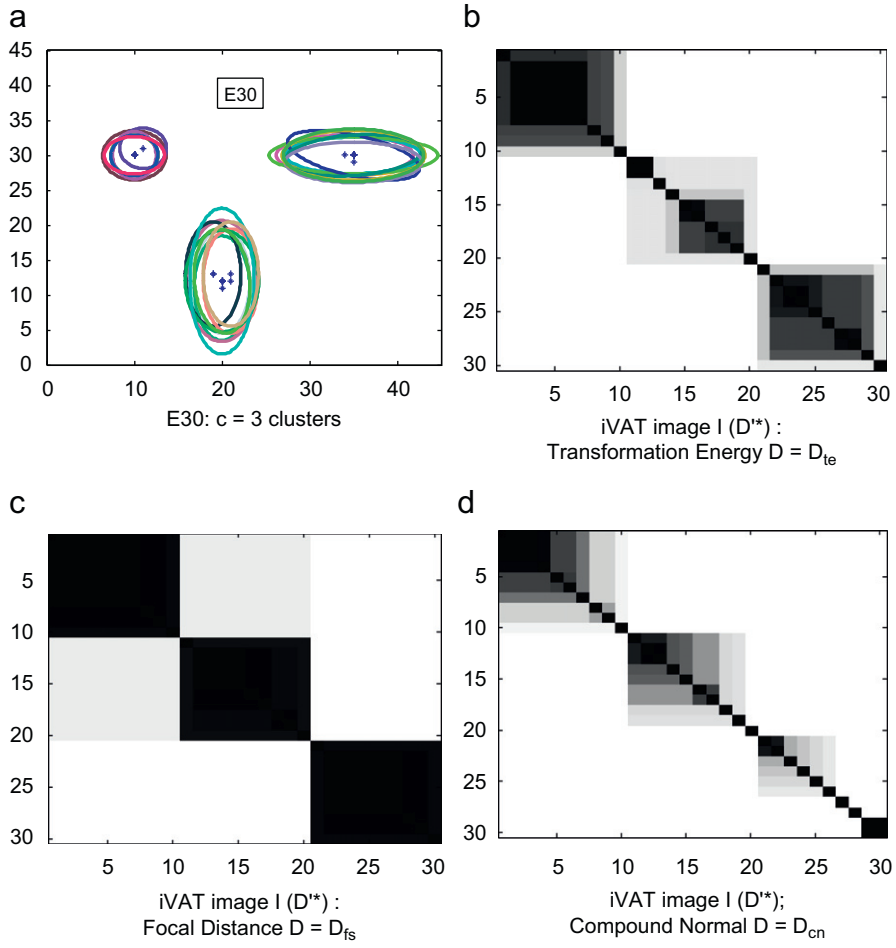

Fig. 8. Data set *E*30 and iVAT images for the three similarity measures.

Example 2. Fig. 8(a) is the data set *E*30, which has, by design, a set of three well-separated clusters, 10 ellipses each. Failure of one of the measures, algorithms or validity indicators on this idealized data will raise a caution flag about its utility for this problem.

The iVAT image in Fig. 8(c) has 3 primary, very dark blocks along its diagonal, each block of size 10×10, strongly suggesting that there are $c=3$ clusters in *E*30. The images in (b) and (c) are much less conclusive. The energy image at (b) has three primary dark blocks, but clearly indicates substructure within each primary cluster. Reading down the diagonal from the top, there are 2, 5, and 3 substructural blocks in (b). The compound image is even less conclusive: its primary structure suggests perhaps 17 clusters. We will be alert for further evidence that these latter two measures are less reliable than focal distance.

Example 3. This example is based on the set *E*40 is shown in Fig. 9a. This is a much more challenging test for our measures. The lower left cluster contains 30 ellipses roughly centered at (12, 15). 15 of these ellipses have a horizontal major axis while the other

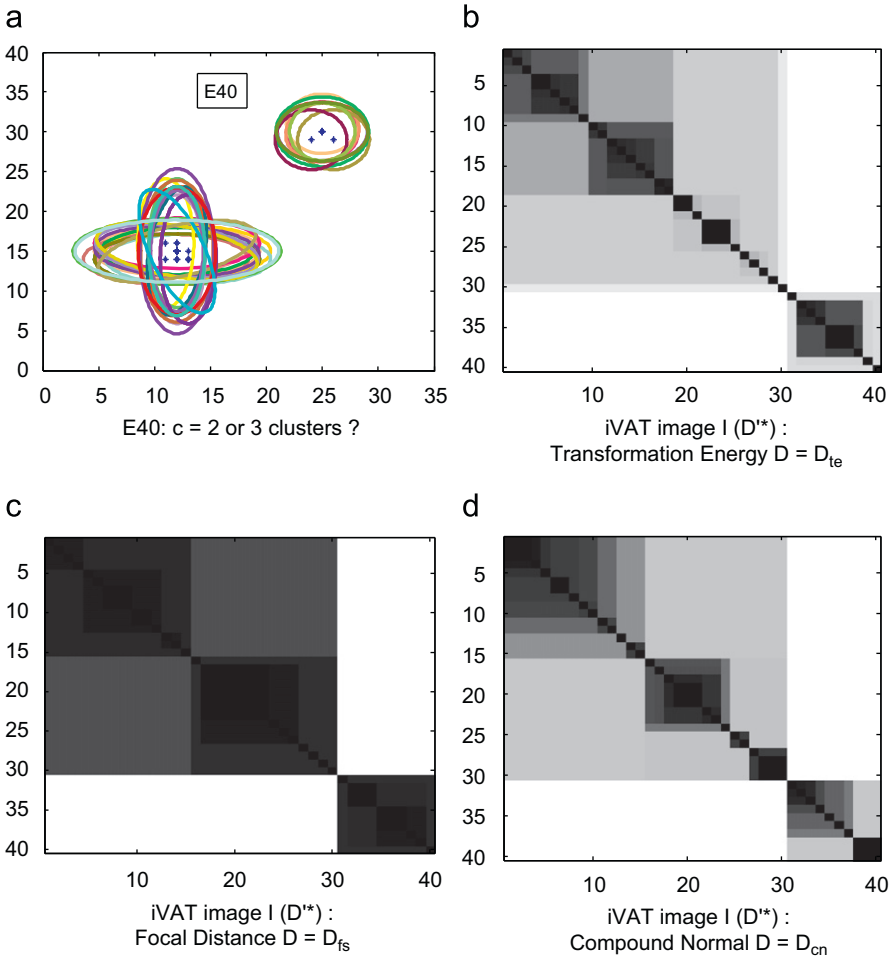

Fig. 9. Data set *E*40 and iVAT images for the three similarity measures.

15 have a vertical major axis. The other cluster, roughly centered at (25, 30), has 10 ellipses that are fairly circular. Many observers see three clusters because of the orientation of the two sets of 15, but other observers see primary cluster structure at $c=2$ because the set of 30 have a strong and similar central tendency. Does the visually apparent structure of *E*40 suggest $c=2$? Or is $c=3$ a better choice?

All three iVAT images suggest that we take $c=2$ for the primary structure in the data. The 30×30 block in the focal distance image (9c) is (albeit faintly) subdivisible into 2 15×15 blocks—that is, $c=3$ is suggested as a secondary interpretation of this data by focal distance. The other two images are quite fragmented beyond their primary implication that $c=2$. We think that $c=2$ and $c=3$ are both acceptable interpretations of *E*40.

Example 4. Fig. 10(a) is a repeat of Fig. 2. Recall that these 54 ellipses represent data collected at the 54 nodes in the IBRL network, and that the "horizontal" ellipse that is visually apparent in this data is atypical node 17. Looking further at these ellipses, you may notice that the ones with axes tilted at roughly -45^{o} have means that are considerably displaced along this direction, and quite a few of them are much shorter than others. So, many of these ellipses may be more dissimilar to their similarly oriented neighbors than to ellipse 17. Nonetheless, the preferred value for this real data is $c=2$, since ellipse 17 is a known second order anomaly in this WSN. Thus, we hope to deduce from visual assessment that these data contain $c=2$ clusters of ellipses.

What do the iVAT images tell us about *E*54? We see *exactly* the structure we are hoping for in Fig. 10(c)—node 17 corresponds to the single dark pixel in the bottom right corner of the focal distance image, the remaining 53 ellipses being the 53×53 block. Moreover, this image reveals a number of substructures within the primary cluster of 53 ellipses, as is borne out by visual examination of the data set. Neither the transformation energy nor the compound normal images in views 10(b) and (d) present a very clear picture of structure in *E*54. The overall results of Examples 2, 3, and 4 suggest that focal similarity s_{fs} provides the "best" iVAT images: they fully agree with the visually apparent clusters in all three data sets. Now we turn to detecting the clusters suggested by these images.

8. Finding clusters in sets of ellipsoids

Looking for clusters in E raises two questions. First, *before* clustering, we must ask how many clusters to look for? Second, *after* clustering, how much credence shall we put on the "optimal" partition of the data? The iVAT images of Section 7 offer visual suggestions for value(s) of c in each of our three test sets prior to clustering. There are many, many other ways to estimate c prior to clustering. The second pre-clustering approach tested here is based on the eigenvalues of D. Ferenc proved in [39] that a nonsymmetric $n\times n$ matrix consisting of c (dark) blocks has c large eigenvalues of order c while the other characteristic values

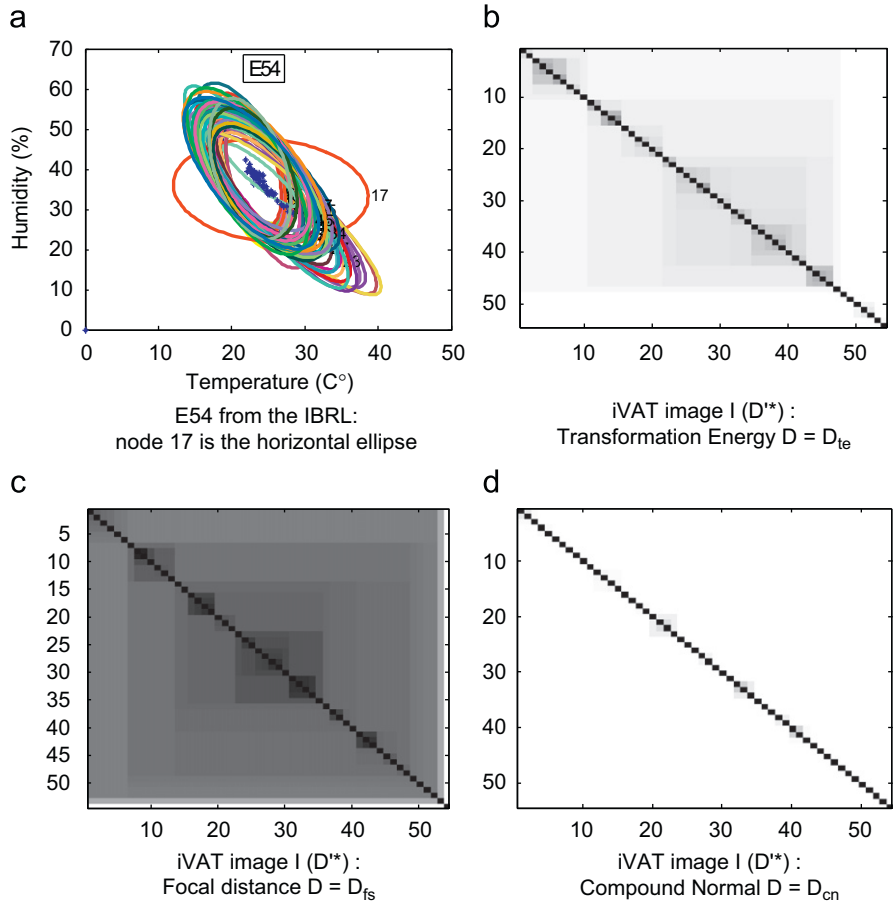

Fig. 10. IBRL data set *E*54 and iVAT images for the three similarity measures.

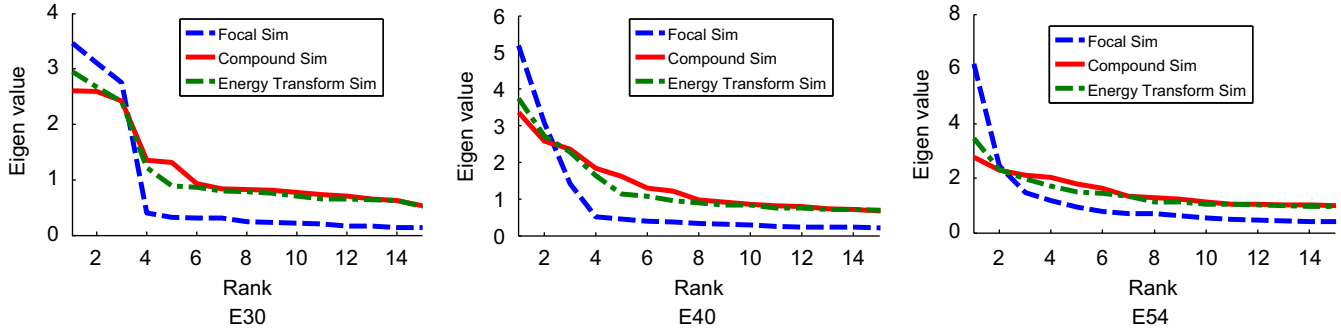

Fig. 11. The largest 15 ordered eigenvalues for each *D* and each data set.

remain of order $\sqrt{n}$ as n tends to infinity. Fallah et al. [40] recently showed that Ferenc's theorem could be used as a *pre-clustering* assessment method to help when choosing the best SL clusters, by looking for a "big jump" in a plot of the square roots of the *ordered eigenvalues* (OEVs) of *D*. (Square roots just improve the visual interpretation of where the big jump occurs.) Note that the theory underlying this strategy is not tied to any clustering algorithm. Fig. 11 shows plots of the first 15 OEVs of each *D* for each of our three data sets.

According to the theory, we expect to find c big eigenvalues, a knee at the big jump, and then a leveling off in the graph for the smaller eigenvalues. The focal similarity graphs have pretty well defined breaks that suggest $c=3$ for all three data sets. It is much harder to see the indicated choices from the graphs of the other two measures, as they are much flatter. The most inconclusive graph is the compound graph for *E*54, which does not really suggest that there are c dominant eigenvalues.

Table 2
Pre-clustering estimates of the best value for c.

Data	c^*	Focal		Energy		Compound	
		iVAT	OEV	iVAT	OEV	iVAT	OEV
*E*30	3	3	3	3	2	**17**	3
*E*40	2/3	2	3	2	**4**	2	**6**
*E*54	2	2	2	2	2	**51**	–

Table 2 lists the pre-clustering best guesses for c for each of our three test sets using the iVAT and OEV methods. Bold values are

incorrect estimates. The column headed "c^*" shows the visually apparent correct number of clusters in each data set. The two methods agree with c^* in 3/9 cases. iVAT indicates the correct c^* for all three data sets using either focal distance or the energy similarity. The compound measure does not provide good estimates of c^* using either the visual (iVAT) or analytic (OEVs) methods.

There are also many ways to look for the clusters in D suggested by iVAT images. Here we discuss two related approaches. One is the well-known *single linkage* (SL) algorithm [16] and the other is the CLODD (*clustering in ordered dissimilarity data*) algorithm [37]. CLODD processes dark block images made by reordering D, while SL processes D directly. These two algorithms are known to produce the same clusters from D under some – but not all – circumstances. Interested readers may consult [38] for a discussion of the theory underlying this relationship.

The classic method for choosing the "optimal" number of clusters found by SL is to look for a "big jump" in the graph of SL merger distances, and back up one step. The heuristic justifying this procedure is that the biggest merger distance indicates the maximum resistance for merger, so the clusters just ahead of this merger are the most desirable. Fig. 12 shows the SL merger distance graphs for $c=15$ to $c=2$ (merging, we plot higher c's to the left). Table 3 shows the values of c identified as optimal by this method, headed as *SLmd* (single linkage merger distance). CLODD has an internal measure of validity—viz., its objective function values. Each validation method has successes and failures (as do all validation indices). The failures are again shown as bold values. We see that the

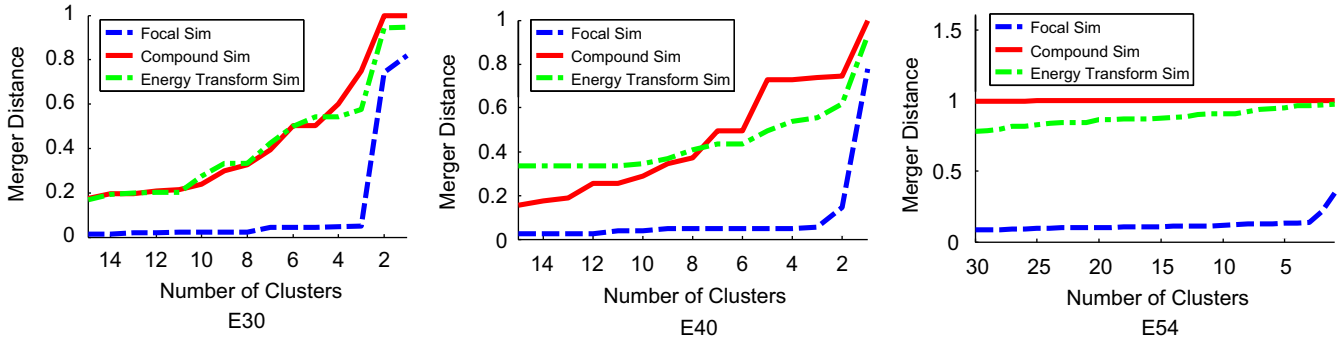

Fig. 12. Plots of SL merger distances for each D and each data set.

Table 3
Post-clustering estimates of the best value for c.

Data	c^*	Focal		Energy		Compound	
		SLmd	CLODD	SLmd	CLODD	SLmd	CLODD
*E*30	3	3	3	**17**	**6**	**10**	**9**
*E*40	2/3	3	2	**21**	**10**	**15**	**11**
*E*54	2	2	2	**51**	**11**	**12**	**11**

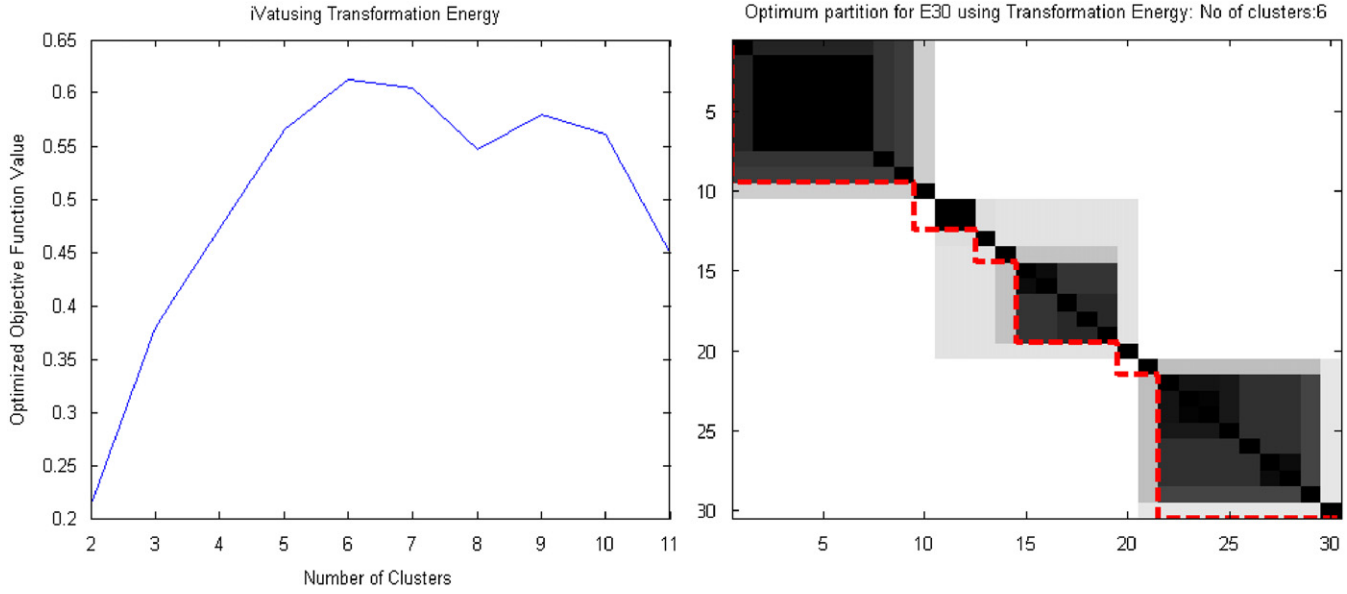

Fig. 13. CLODD objective function and partition extracted from the energy transform iVAT image of *E*30.

preferred SL and CLODD partitions agree with c^* in all three tries only for the focal distance measure. Most importantly, the optimal SL partitions of all three data sets agree with visual assessment of the input data when focal similarity is used to build the input dissimilarity data, and this method is the only one that recovers the apparently correct answer for the WSN data *E*54.

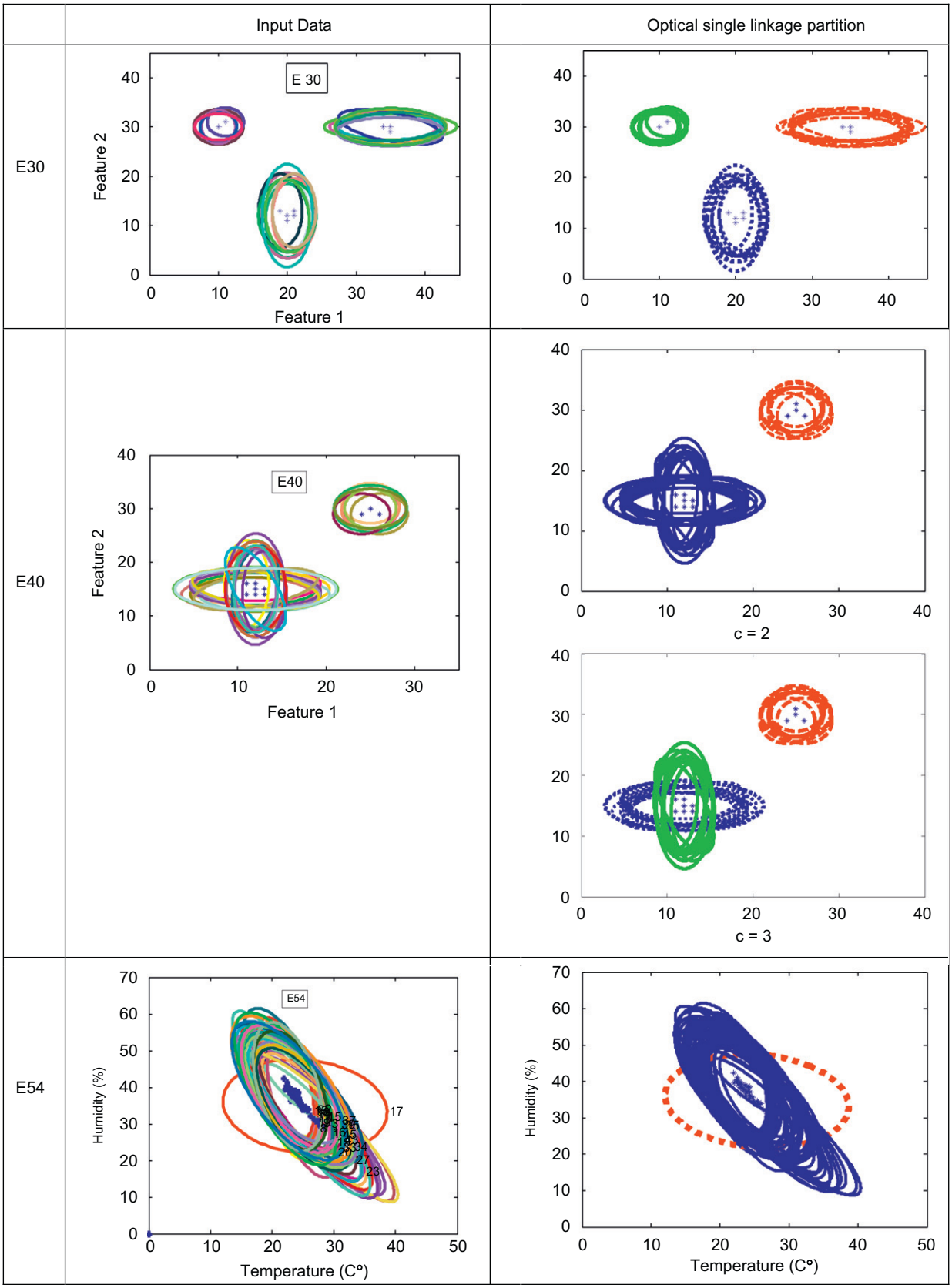

Fig. 14. Optimal single linkage partitions of the data sets based on the focal similarity measure.

Table 4
The procedures used in this paper.

Data collection	Build 3 measures	Pre-clustering assessment (to estimate c)	Find partitions $\{U\}$ of ellipse data	Post-clustering validation (choose best U)
Synthetic data $E30$ and $E40$	Focal distance	OEVs of D	Single linkage applied to D	Biggest jump in SL merger distance
Real IBRL data $E54$	Transformation energy	iVAT image $I(D'^{*})$	CLODD applied to $I(D'^{*})$	Maximum value of CLODD function
	Compound normalized			

CLODD processes reordered images directly. CLODD is run on D for $c=2, 3, \ldots, c_{max}$, and the optimal partition of c is taken as the one that maximizes the CLODD objective function. Table 3 shows the values that CLODD chooses as optimal based on its objective function. CLODD recovers the desired clusters in 3/9 tries, so it seems less effective than SL for this application. Bear in mind, however, that CLODD extracts clusters from the iVAT image $I(D'^{*})$ by identifying the best fit of its objective function to the dark block structure in the image. Thus, when an iVAT image seems to have imbedded substructure in its primary dark blocks, CLODD will extract a partition corresponding to this visual structure. Fig. 13 is an example of CLODD applied to the iVAT image of $E30$ based on the energy transform similarity. The left view shows a plot of the CLODD objective function, which maximizes at $c=6$. The right view is the optimal partition extracted by CLODD at this value of c. The dotted red lines indicate the boundaries of the partition. We point out that, unlike SL, which has no "tuning parameters", CLODD has several user-defined parameters that can be adjusted to alter model performance.

Finally, Fig. 14 displays the three data sets and the optimal single linkage partitions of each. As you can see, there seems to be perfect agreement between the clusters obtained by single linkage and the visually apparent clusters in the data. The corresponding partitions based on the energy transform were the same as those for $E30$ and $E40$, but the optimal solution at $c=2$ for $E54$ identified the smallest of the 53 aligned ellipses in the data as the singleton. Optimal SL partitions based on the compound similarity matched the ones in Fig. 11 only on $E30$. Fig. 14 also displays the single linkage partition at $c=2$ for $E40$. This is the primary partition that is suggested by the iVAT image of $E40$ in view 9(c). This partition is also the one found at $c=2$ by applying single linkage to the other two matrices of dissimilarity, so this interpretation of the data is compelling. The results shown in Fig. 14 corroborate our earlier assertion that focal distance is the most reliable of the three measures. Using the focal distance dissimilarity matrix results in the correct partitioning of the input data by single linkage clustering in all three tests.

9. Conclusions and discussion

First, we defined and analyzed three measures of similarity for pairs of hyperellipsoids in p-space. Then we introduced a way to visually assess cluster substructure in sets of ellipses using the recursive iVAT algorithm to reorder dissimilarity data set $D \rightarrow D'^{*}$. The reordered image $I(D'^{*})$ shows clustering tendencies in the objects underlying D as dark sub-blocks along the main diagonal. We introduced a second pre-clustering assessment method based on the ordered eigenvalues (OEVs) of D. Our examples confirmed that the visual assessment of possible clusters in dissimilarity data with iVAT is consistent with the theoretically sound OEV analytic approach. Finally, we presented three numerical examples using data sets: $E30$—comprising 3 well separated subsets of 10 synthetic ellipses; $E40$—a set of 40 synthetic ellipses having 2 primary and 3 secondary clusters; and $E54$—a set of real WSN data that had one second order node anomaly and 53 normally operating sensor nodes. We found clusters in these three data sets using the single linkage and CLODD clustering algorithms, and assessed the clustering results with two methods: big jumps in the SL merger distances and maxima of the CLODD objective function. A number of things were discussed in this paper. It might be helpful to refer to Table 4 for a graphic depiction of the procedures used.

The three examples presented in this paper are pretty strong evidence for the following assertions: (i) for these data sets, the focal similarity is very effective, while the transformation energy and compound normal measures are both unreliable; (ii) when the ellipses are used to build a dissimilarity matrix D with the focal distance, iVAT provides accurate visual estimates of c that agree with the ordered eigenvalues of D for clusters of ellipsoids; (iii) single linkage reliably extracts the clusters of ellipsoids suggested by iVAT images. As is the case with *all* pattern recognition models, there will be instances where these assertions are false, but we think that our examples show that the suggested model has enough merit to warrant further study.

What's next? Perhaps the most important extension of this initial study concerns the efficacy of our methodology for "real" hyperelllipsoids. Although the three measures developed in this paper are well defined for any value of p, we have not tested this scheme for elliptical data summaries when $p>2$. But there are already WSNs that collect $p=3$, 4, and 5 measurements at each station [10], and the number of measured features is certain to grow as sensor technology improves the hardware available for WSNs. Our intuition is that for p much larger than 3 or 4, these measures will be inadequate unless n, the number of ellipsoids, is many thousands. If this is the case, some way to usefully extend these ideas to higher dimensions will be required.

References

[1] R.A. Johnson, D.A. Wichern, Applied Multivariate Statistical Analysis, 3rd ed, Prentice-Hall, Englewood Cliffs, NJ, 1992.
[2] P.M. Kelly, D.R. Hush, J.M. White, An adaptive algorithm for modifying hyperellipsoidal decision surfaces, J. Artif. Neural Networks 1 (4) (1994) 459–480.
[3] P.M. Kelley, An algorithm for merging hyperellipsoidal clusters (1994). TR LA-UR-94-3306, Los Alamos National Laboratory, Los Alamos, NM, 1994.
[4] R.N. Davé, K.J. Patel, Fuzzy ellipsoidal-shell clustering algorithm and detection of elliptical shapes, in: D.P. Casasent (Ed.), SPIE Proceedings of the Intelligent Robots and Computer Vision IX, vol. 1607, 1991, pp. 320–333.
[5] Y. Nakamori, M. Ryoke, Identification of fuzzy prediction models through hyperellipsoidal clustering, IEEE Trans. Syst. Man Cybernet. 24 (8) (1994) 1153–1173.
[6] J. Dickerson, B. Kosko, Fuzzy function learning with covariance ellipsoids, in: Proceedings of the IEEE International Conference on Neural Networks, IEEE Press, Piscataway, NJ, 1993, pp. 1162–1167.
[7] R. Duda, P. Hart, Pattern Classification and Scene Analysis, Wiley Interscience, New York, 1973.
[8] S. Rajasegarar, C. Leckie, M. Palaniswami, CESVM: centered hyperellipsoidal support vector machine based anomaly detection, in: Proceedings of the IEEE ICC 2008, 2008, pp. 1610–1614.
[9] S. Rajasegarar, J.C. Bezdek, C. Leckie, M. Palaniswami, Analysis of anomalies in IBRL data from a wireless sensor network deployment, in: Proceedings of the

International Conference on Sensor Technologies and Applications, 2007, pp. 158–163.
[10] S. Rajasegarar, J.C. Bezdek, C. Leckie, M. Palaniswami, Elliptical anomalies in wireless sensor networks, ACM TOSN 6 (1) (2009) 1550–1579.
[11] M. Moshtaghi, S. Rajasegarar, C. Leckie, S. Karunasekera, Anomaly detection by clustering ellipsoids in wireless sensor networks, in: Proceedings of the Fifth International Conference on Intelligent Sensors, Sensor Networks and Information Processing (ISSNIP 2009), 7–10 December 2009, Melbourne, Australia, 2009.
[12] J.C. Bezdek, T.C. Havens, J.M. Keller, C.A. Leckie, L Park, M. Palaniswami, S. Rajasegarar, Clustering elliptical anomalies in sensor networks, in Proceedings of the FUZZ-IEEE, Barcelona, 2010.
[13] H.Y.T Ngan, G.K.H. Pang, N.H.C. Yung, Ellipsoidal decision regions for motif-based patterned fabric defect detection, Pattern Recog. 43 (2010) 2132–2144.
[14] J.C. Bezdek, R.J. Hathaway, VAT: a tool for visual assessment of (cluster) tendency, in: Proceedings of the 2002 International Joint Conference on Neural Networks, Honolulu, HI, 2002, pp. 2225–2230.
[15] T.C. Havens, J.C. Bezdek, A recursive formulation of the Improved Visual Assessment of Cluster Tendency (iVAT) Algorithm, IEEE TKDE, in review.
[16] S. Theodoridis, K. Koutroumbas, Pattern Recognition, 5th ed., Academic Press, New York, 2010.
[17] J.C. Bezdek, J.M. Keller, R. Krishnapuram, N.R. Pal, Fuzzy Models and Algorithms for Pattern Recognition and Image Processing, Kluwer, Norwell, 1999.
[18] A. Jain, R. Dubes, Algorithms for Clustering Data, Prentice Hall, Englewood Cliffs, NJ, 1988.
[19] J. Hartigan, Clustering Algorithms, Wiley, New York, 1975.
[20] R. Xu, D.C. Wunsch, Clustering, IEEE Press, Piscataway, NJ, 2009.
[21] I. Borg, J. Lingoes, Multidimensional Similarity Structure Analysis, Springer-Verlag, New York, NY, 1987.
[22] E.R. Tufte, The Visual Display of Quantitative Information, 2nd ed, Graphics Press, Cheshire, CT, 2001.
[23] I.H. Witten, E. Frank, Data Mining: Practical Machine Learning Tools and Techniques, 2nd ed, Morgan Kaufmann, San Francisco, CA, 2005.
[24] T. Soukup, I. Davidson, Visual Data Mining: Techniques and Tools for Data Visualization and Mining, Wiley, New York, NY, 2002.
[25] B.S. Everitt, Graphical Techniques for Multivariate Data, North Holland, New York, 1978.
[26] R.C. Tryon, Cluster Analysis, Edwards Bros., Ann Arbor, MI, 1939.
[27] R.B. Cattell, A note on correlation clusters and cluster search methods, Psychometrika 9 (1944) 169–184.
[28] P.H.A. Sneath, A computer approach to numerical taxonomy, J. Gen. Microbiol. 17 (1957) 201–226.
[29] G.D. Floodgate, P.R. Hayes, The Adansonian taxonomy of some yellow pigmented marine bacteria, J. Gen. Microbiol. 30 (1963) 237–244.
[30] R.F. Ling, A computer generated aid for cluster analysis, Commun. ACM 16 (1973) 355–361.
[31] J.C. Bezdek, R.J. Hathaway, VAT: a tool for visual assessment of (cluster) tendency, in: Proceedings of the IJCNN 2002, IEEE Press, Piscataway, NJ, 2002 pp. 2225–2230.
[32] R.J. Hathaway, J.C. Bezdek, J.M. Huband, Scalable visual assessment of cluster tendency for large data sets, Pattern Recogn. 39 (2006) 1315–1324.
[33] J.C. Bezdek, R.J. Hathaway, J.M. Huband, Visual assessment of clustering tendency for rectangular dissimilarity matrices, IEEE Trans. Fuzzy Sys. 15 (5) (2007) 890–903.
[34] L. Wang, T. Nguyen, J.C. Bezdek, C.A. Leckie, K. Ramamohanarao, iVAT and aVAT: enhanced visual analysis for cluster tendency assessment, in Proceedings of the PAKDD, Hyderabad, India, June 2010.
[35] T.C. Havens, J.C. Bezdek, A recursive formulation of the Improved Visual Assessment of Cluster Tendency (iVAT) Algorithm, IEEE TKDE, in review.
[36] N.R. Conn, N.I.M. Gould, Ph.L. Toint, Trust-Region Methods, MPS/SIAM Series on Optimization, SIAM and MPS, 2000.
[37] T.C. Havens, J.C. Bezdek, J.M. Keller, M. Popescu, Clustering in ordered dissimilarity data, Int. J. Intell. Sys. 24 (5) (2008) 504–528.
[38] T.C. Havens, J.C. Bezdek, J.M. Keller, M. Popescu, J.M. Huband, Is VAT really single linkage in disguise? Ann. Math. Artif. Intell. 55 (3–4) (2009) 237–251.
[39] Juhfisz Ferenc, On the characteristic values of non-symmetric block random matrices, J. Theoret. Probab. 3 (2) (1990) 199–205.
[40] S. Fallah, D. Tritchler, J. Beyene, Estimating number of clusters based on a general similarity matrix with application to microarray data, Statist. Appl. Genet. Mol. Biol. 7 (1) (2008) 1–23.

Masud Moshtaghi received his B.Sc. degree in 2006 in computer science, and his M.S. in software engineering in 2008 from the University of Tehran. He has been with the University of Melbourne from March 2009. His research interests include pattern recognition, artificial intelligence for network security, data mining, and wireless sensor networks.

Timothy C. Havens received his M.S. degree in electrical engineering from Michigan Tech University in 2000. After that, he was employed at MIT Lincoln Laboratory where he specialized in the simulation and modelling of directed energy and global positioning systems. In 2006, he began work on his Ph.D. degree in electrical and computer engineering at the University of Missouri. His interests include clustering in relational data and ontologies, fuzzy logic, and bioinformatics but, by night, he is a jazz bassist.

James C. Bezdek received his Ph.D. in Applied Mathematics from the Cornell University in 1973. Jim is the past president of NAFIPS (North American Fuzzy Information Processing Society), IFSA (International Fuzzy Systems Association) and the IEEE CIS (Computational Intelligence Society): founding editor of the Int'l. Jo. Approximate Reasoning and the IEEE Transactions on Fuzzy Systems: Life fellow of the IEEE and IFSA; and a recipient of the IEEE 3rd Millennium, IEEE CIS Fuzzy Systems Pioneer, and IEEE Technical Field Award Rosenblatt medals. Jim's interests: woodworking, optimization, motorcycles, pattern recognition, cigars, clustering in very large data, fishing, co-clustering, blues music, wireless sensor networks, poker, and visual clustering. Jim retired in 2007, and will be coming to a university near you soon.

Laurence Park received his B.E. (Hons.) and B.Sc. degrees from the University of Melbourne, Australia in 2000 and Ph.D. degree from the University of Melbourne in 2004. He joined the Computer Science Department at the University of Melbourne as a Research Fellow in 2004, and was promoted to Senior Research Fellow in 2008. Laurence joined the School of Computing and Mathematics at the University of Western Sydney as a Lecturer in Computational Mathematics and Statistics in 2009, where he is currently investigating methods of large scale data mining and machine learning. During this time, Laurence has been made an Honorary Senor Fellow of the University of Melbourne.

Christopher Leckie is an Associate Professor and Deputy-Head of the Department of Computer Science and Software Engineering at the University of Melbourne in Australia. A/Prof. Chris Leckie has over two decades of research experience in artificial intelligence (AI), especially for problems in telecommunication networking, such as data mining and intrusion detection. A/Prof. Leckie's research into scalable methods for data mining has made significant theoretical and practical contributions in efficiently analyzing large volumes of data in resource-constrained environments, such as wireless sensor networks.

Sutharshan Rajasegarar received his B.Sc. Engineering degree in Electronic and Telecommunication Engineering (with first class honours) in 2002, from the University of Moratuwa, Sri Lanka, and his Ph.D. in 2009 from the University of Melbourne, Australia. He is currently a Research Fellow with the Department of Electrical and Electronic Engineering, The University of Melbourne, Australia. His research interests include wireless sensor networks, anomaly/outlier detection, machine learning, pattern recognition, signal processing, and wireless communication.

James M. Keller received his Ph.D. in Mathematics in 1978. He holds the University of Missouri Curators' Professorship in the Electrical and Computer Engineering and Computer Science Departments on the Columbia campus. He is also the R. L. Tatum Professor in the College of Engineering. His research interests center on computational intelligence: fuzzy set theory and fuzzy logic, neural networks, and evolutionary computation with a focus on problems in computer vision, pattern recognition, and information fusion including bioinformatics, spatial reasoning in robotics, geospatial intelligence, sensor and information analysis in technology for eldercare, and landmine detection. His industrial and government funding sources include the Electronics and Space Corporation, Union Electric, Geo-Centers, National Science Foundation, the Administration on Aging, The National Institutes of Health, NASA/JSC, the Air Force Office of Scientific Research, the Army Research Office, the Office of Naval Research, the National Geospatial Intelligence Agency, the Leonard Wood Institute, and the Army Night Vision and Electronic Sensors Directorate. Professor Keller has coauthored over 350 technical publications. Jim is a Fellow of the Institute of Electrical and Electronics Engineers (IEEE) for whom he has presented live and video tutorials on fuzzy logic in computer vision, is an International Fuzzy Systems Association (IFSA) Fellow, an IEEE Computational Intelligence Society Distinguished Lecturer, a national

lecturer for the Association for Computing Machinery (ACM) from 1993 to 2007, and a past President of the North American Fuzzy Information Processing Society (NAFIPS). He received the 2007 Fuzzy Systems Pioneer Award from the IEEE Computational Intelligence Society. He finished a full six year term as Editor-in-Chief of the IEEE Transactions on Fuzzy Systems, is an Associate Editor of the International Journal of Approximate Reasoning, and is on the editorial board of Pattern Analysis and Applications, Fuzzy Sets and Systems, International Journal of Fuzzy Systems, and the Journal of Intelligent and Fuzzy Systems. Jim was the Vice President for Publications of the IEEE Computational Intelligence Society from 2005 to 2008, and is currently an elected Adcom member. He was the conference chair of the 1991 NAFIPS Workshop, program co-chair of the 1996 NAFIPS meeting, program co-chair of the 1997 IEEE International Conference on Neural Networks, and the program chair of the 1998 IEEE International Conference on Fuzzy Systems. He was the general chair for the 2003 IEEE International Conference on Fuzzy Systems.

Marimuthu Palaniswami received his M.E. from the Indian Institute of Science, India, M.Eng.Sc. from the University of Melbourne and Ph.D. from the University of Newcastle, Australia before rejoining the University of Melbourne. He has published over 340 refereed research papers. He currently leads one of the largest funded ARC Research Network on Intelligent Sensors, Sensor Networks and Information Processing (ISSNIP) programme—that is structured it run as a network centre of excellence with complementary funding for fundamental research, test beds, international linkages and industry linkages. His leadership includes as an external reviewer to an international research centre, a selection panel member for senior appointments/promotions, grants panel member for NSF, advisory board member for European FP6 grant centre, steering committee member for NCRIS GBROOS and SEMAT, and board member for IT and SCADA companies. His research interests include SVMs, Sensors and Sensor Networks, Machine Learning, Neural Network, Pattern Recognition, Signal Processing and Control.